**Journal of Mines, Metals and Fuels,** 71(6): 811-828; 2023. DOI: 10.18311/jmmf/2023/34498

Print ISSN : 0022-2755

Journal of Mines, Metals and Fuels

Contents available at: www.informaticsjournals.com/index.php/jmmf

# Performance Evaluation of Blended Wing Body Aircraft Using Numerical Techniques

**Vanshika Gupta[1] and Srinivas G[1*]**

*[1]Department of Aeronautical & Automobile Engineering, Manipal Institute of Technology, Manipal Academy of Higher Education (MAHE), Manipal, Udupi, Karnataka, India 576104. E-mail: srinivas.g@manipal.edu*

## Abstract

*The ever-increasing demands of humanity have given rise to numerous innovative technological advances in each and every field throughout history. Aviation is one such field, and future demands in air transportation, such as noise reduction, improved aerodynamic performance, lower operating costs, higher fuel efficiency, and so on, led aircraft designers to conceptualize the Blended Wing Body (BWB). The BWB has proven to be more aerodynamic and efficient than conventional designs. This paper attempted to evaluate BWB performance using various numerical techniques. This study aims to contribute to the emerging research in this field by verifying previous results on a baseline BWB design and improving them through numerical model optimization. The baseline BWB model has been numerically simulated at various angles of attack ranging from 0º to 40º and low subsonic Mach numbers to determine its, lift to drag ratio, and thus its aerodynamic efficiency under these conditions. The baseline model has been modified by adding winglets, and changing the sweep angle and airfoil used for the outer wing. For this optimized model, numerical simulations with boundary conditions similar to the baseline have been run, and the results have been compared and validated with the baseline. All numerical simulations of the BWB vehicle were thoroughly investigated, including flow properties such as pressure, temperature, density, turbulence model, and so on. The results of this study have also been compared to a traditional flight to highlight the enhancements in the aerodynamic performance provided by the BWB configuration.*

**Keywords:** *Blended wing body (BWB), Computational fluid dynamics (CFD), Aerodynamic efficiency, Drag coefficient, Angle of attack*

## 1.0 Introduction

Based on the earlier flying wing aircraft concept, the non-conventional blended wing body configuration was developed which integrates the fuselage and the wing, while eliminating the tail and thus the horizontal stabilizer and rudder from the aircraft[37]. This configuration of the BWB allows for a reduction in the wetted area and interference drag, which in turn increases the maximum L/D ratio by 20% and thus the performance of the aircraft. The effective surface area contributing to the lift is more than that of a conventional design as the fuselage of the BWB generates lift together with the wings of the aircraft[35]. The removal of the tail also significantly reduces the surface area leading to a reduction in drag[43]. Other noteworthy advantages of this shape are 27% lesser fuel burn, a 15% decrease in take-off weight, and a 27% reduction in total thrust[18].

The load and weight distribution are more even for a BWB, and thus it is capable of carrying more cargo weight and increased number of passengers as compared to the conventional design[42]. According to a study conducted on Airbus A380, 550 passengers can be accommodated in its twin deck comfortably[20]. However, 800 passengers can be carried along with lesser fuel consumption if the BWB design

*Author for correspondence

is implemented, which will in turn reduce the direct operating cost of the aircraft. The BWB does not require any trailing or leading-edge devices for flaps or tailplanes for pitch control during take-off or landing. This leads to a reduction in the noise signatures for BWB[36]. A significant improvement has also been observed in the cost-per-seat-mile[18]. Other than that, fewer pollutants are emitted by the BWB as a result of lower fuel burn and higher propulsive efficiency.

Despite having the above-listed advantages which make the BWB design superior to the conventional TAW configuration, at present, there are a few limitations as well that reduce the feasibility of the BWB configuration replacing the traditional design[41]. Thus, new concepts, design optimization techniques, and evolved technologies are being developed through increased research activities for the BWB to overcome these challenges and make it more feasible for commercial air transportation[34].

In the present study, a BWB model is designed based on previous works[30,14]. The baseline and a modified model have been numerically simulated using Ansys FLUENT, and the aerodynamic flow behaviour has been studied at varying angles of attack. This study aims to contribute to the evolving field of BWB and thus the future of commercial air transportation.

Figure 1: Boeing X-48C BWB (Google, n.d.)

# 2.0 Literature Review

## 2.1 Origin of the BWB Concept

For the past 35 years, research on the BWB concept is being conducted, owing to the numerous advantages they offer over the conventional design. It all started when Dennis Bushnell of NASA's Langley Research center challenged the academia raising the question "Is there a renaissance for the long-haul transport?"[18]. This led to the realization of the future demands of air transportation that the conventional TAW aircraft could not achieve, i.e., noise reduction, fuel efficiency, improved aerodynamic performance, payload/passenger capacity, etc.

R. H. Liebeck summarized, analyzed, and traced the development of this model in his various publications. In his 1997 publication, he illustrated the design process and technical challenges faced by the then-novel BWB configuration[37]. It was concluded that the centerbody region could be designed using thick airfoils, allowing for more cabin space and minimal profile drag along with reduced wave drag resulting from strong, unswept shocks. A comparison of the 800 passengers, 7000 nautical miles range BWB configuration, and conventional design with comparable specifications was conducted by him in 1998[17]. 27% reduced fuel burn, 15% reduction in take-off weight, 12% reduced operating empty weight, and 27% lower total thrust was observed for the BWB design when compared to the conventional design. In addition to this, an increment of 20% was observed for the L/D ratio. Liebeck demonstrated the design limitations and challenges faced by the BWB through his 2003 publication[15]. Here, the challenge of identifying the optimal design cruise Mach number, flight mechanics, and size and application commonality of the BWB concept has been discussed. In the year 2004, Liebeck chronicled the technical progress of the BWB concept over the years[16].

Martínez-Val et. al. studied the flying wing aircraft configuration extensively[23]. Another one of their publications from 2007 discusses the issue of trailing edge vortices that are shed by the flying wing during flight[11]. His 2020 publication provides a thorough overview of the flying wing aircraft, discussing its main features, advantages over the conventional design, and important challenges like vortex wake and evacuation[22].

## 2.2 Advantages of BWB over the Traditional TAW Configuration

A BWB aircraft, when compared to a conventional aircraft, has a high lift to drag ratio, is lighter, burns lesser fuel, has lower operating costs, is structurally more efficient, emits lesser pollutants, has lower noise signatures, and has a higher payload or passenger-carrying capacity[40].

In 2010, Martínez-Val et. al. found a 7 to 10 dB noise reduction for a flying wing aircraft approaching the airport when compared to the conventional design[24]. Hill and Thomas, studied different configurations of aircrafts intending to improve noise emitted using integration of propulsion airframe (PAA)[13]. A conceptual design methodology for BWB was developed by Brown and Vos in the year 2018[8]. The operating empty weight was predicted to be lower for the BWB design, which in turn results in lower fuel burn per passenger-kilometers.

A BWB aircraft is capable of achieving optimum lift coefficients at relatively higher angles of attack as compared to the traditional aircraft[10]. Velázquez et al., in their 2017 publication, conducted CFD analysis on a BWB aircraft under the stall and low-speed approach conditions[44]. Midhun et al. performed experimental and numerical investigations on a small-sized BWB model[28]. Both results showed that the aircraft can fly at high angles of attack ($\alpha$=45º) before stalling. Chen et al., 2019[9], studied the technological developments in the field of BWB aircraft through the years. The BWB aircraft have a high aerodynamic efficiency owing to its larger mean aerodynamic chord, increased wetted aspect ratio, and the flight Mach number. The BWB configuration has been proved to be around 31.5% more fuel-efficient.

## 2.3 Limitations and Challenges Faced by the BWB Aircraft

Although they have numerous advantages and potential, as discussed in the subheading 2.2, BWB aircraft is still not feasible for implementation as commercial aircraft. This is due to quite a few limitations and challenges that are currently being faced by them. Cabin pressurization, trim, stability, and control issues because of it being a tailless configuration, manufacturing difficulties, low aspect ratio fuselage, passenger acceptance, propulsion system integration, etc. remain some of the major concerns in this field.

Liebeck discussed the design challenges faced by the BWB in his 2003 publication[15] and listed the challenges and areas of risk in his 2004 publication[16], where he also chronicled the work done on the BWB design over the years. The issues and areas of risk are tabulated in Table 1.

Marino and Sabatini discussed the benefits and challenges of the BWB configuration, including passenger acceptance and perception of the design[21]. The internal cabin design must be considered as a priority in order to avoid passenger discomfort[38]. Additionally, new emergency procedures will have to be studied and incorporated as the standard ones will not apply.

While these challenges limit the scope of the BWB configuration, it remains superior to the conventional TAW design in a lot of ways. More research and optimization studies, in an attempt to overcome these challenges, are being conducted to make this design feasible for implementation as commercial air transportation.

## 2.4 Aerodynamic Optimization Studies

Qin et al. conducted a study of trim considerations for a given BWB design in 2004[39]. An inverse twist design approach was used, which led to an improvement in the performance of the model, while also including trim conditions as a design constraint. Peigin and Epstein

**Table 1: Issues and areas of risk (from Douglas aircraft Co., 1995) (Liebeck, 2004)**

| | Issues and areas of risk |
|---|---|
| 1 | Complex flight control architecture and allocation, with severe hydraulic requirements |
| 2 | Large auxiliary power requirements |
| 3 | A new class of engine installation |
| 4 | Flight behaviour beyond stall |
| 5 | High floor angle on approach to take-off and landing |
| 6 | Acceptance by the flying public |
| 7 | Performance at long range |
| 8 | Experience and database for a new class of configuration limited to military aircrafts |

conducted optimization studies on a blended wing body configuration to minimize the total drag[36]. A multi-constrained optimization technique was used for this study. It was found through analysis of the results that this optimization produces an aerodynamic performance very close to what is considered optimum.

An aerodynamic analysis was conducted by Wisnoe et al. in 2009 on a model at Mach 0.3 and a 1/6 half model of the BWB was tested in a wind tunnel at Mach 0.1[45]. The lift, drag, and moment coefficients were compared at both the Mach numbers with respect to variation in the angle of attack. This study revealed that a BWB model of this type is capable of flying at very high Mach numbers, with the maximum lift at around 34º and 39º. The wing stalls at $\alpha$=8º and hence the improvement of the wing is suggested in order to delay flow separation. A redesigned model of the BWB known as ‘Baseline-II’ was introduced in 2010[27] which featured a canard and a relatively slimmer body for the aircraft while preserving the same wingspan. A higher angle of stall ($\alpha$=42º) was obtained with a maximum lift of 1.1. A further study on the static stability and aerodynamics performance of canards for the Baseline-II BWB was conducted by Rizal et al. in 2012[3], where they discovered that if a suitable canard setting angle is found, it can add more lift than drag to the aircraft. Ali et al. in 2011[4] studied the aerodynamic behaviour of the Baseline-II-E2 model without a canard. A linear variation is observed from $\alpha$ = -10º to 7º, changing into non-linear as the angle of attack increases.

In 2014, Lyu and Martins conducted a series of RANS-based shape optimizations on BWB using computational fluid dynamics, to study the balance between the aerodynamic performance, stability, trim and bending moment of a BWB configuration[14]. The fifth case explored the addition of planform variables, where the span was increased by 3% and the sweep angle was decreased by 4º. An additional reduction in drag was observed for this case. A sixth case was also studied, where a multipoint design optimization technique was used to modify the BWB design. As compared to single-point optimizations, the resulting design of this case was more robust.

The stability and control surfaces for a BWB aircraft were studied by Martinez et al.[25] to create a new analysis and designing tool for unconventional aircrafts such as the BWB. A reduction of 12% was obtained in the area of the control surfaces of the baseline model along with a reduction in the weight and drag of the aircraft. Flow analysis of an optimized BWB model was studied through CFD simulations conducted on Ansys FLUENT[26]. The optimization was done using standard optimization techniques to get a better L/D ratio, by changing some of the parameters like the sweep angle, taper ratio, wing twist, etc. Arokkiaswamy & Nishanth P. compared the aerodynamic efficiency of a basic BWB design, a Boeing 747, and an optimized BWB design under the same experimental conditions[6]. A 30% increase in $(C_1)$max, 50% reduction in $(C_d)$max and 30% increase in (L/D)max were observed for the optimized model.

## 2.5 Summary

The blended wing body configuration is considered an innovative breakthrough as it can generate more lift than a conventional aircraft for the same wingspan. It is found to have numerous advantages over the conventional design when it comes to vehicle efficiency, fuel burn, take-off weight, payload capacity, etc. About 60% of the lift is generated by the fuselage of the BWB unlike the fuselage of the conventional design which has no aerodynamic contribution to the lift produced. The blended wing of the BWB configuration leads to a reduction in the wetted area of the aircraft thus increasing its aerodynamic efficiency.

Despite having numerous advantages over the conventional design, the BWB still requires a lot of enhancement to be implemented as a commercial aircraft. The tail elimination has a downside as it leads to stability issues, particularly during pitching as balancing out the moments due to pressure distribution over the airfoils becomes difficult[42]. Pressurization of the cabin of a BWB is also a complication being faced. It is much easier to pressurize the cylindrical cabin of a conventional flight as compared to the BWB[5]. Other than this, it may be difficult on the part of the passengers to accept the BWB configuration as a commercial flight because of the unconventional design, no personal window, and the possibility of motion sickness for the passengers sitting further away from the center.

Currently, research is being conducted on the BWB

Figure 2: Boeing X48–B (Source – Google Images)

Figure 3: Airbus - MAVERIC (Airbus, 2020)

configuration by Airbus (Figure 3) and Boeing (Figure 2) in an attempt to make this design compatible with commercial air transportation. Boeing Phantom Works along with NASA developed the BWB aircraft X-48B, which took its first test flight in 2007. It presented proof of the aerodynamic concept of the BWB and its supremacy over traditional flight. Airbus is also working on a BWB design of its own. MAVERIC, a BWB aircraft scaled demonstrator developed by Airbus, is their most recent advancement in this field[1].

## 2.6 Research Gaps

While many studies have been dedicated to the BWB concept, there are a lot of unknown territories yet to be covered in this field before its implementation as commercial air transport. A few gaps in the research, listed in the following points, have been identified while conducting the literature survey. There is a lack of research on the correlation between real-life flight tests and virtual tests for the BWB. Experimental and numerical results can be better analyzed for accuracy if data from the actual flight test is compared to the experimental data. Moreover, a grid independence test is important to verify the dependency of the results on the grid size of the domain. Little research exists where such tests have been conducted and so more studies should conduct these tests to verify the accuracy of their CFD results.

## 3.0 Objectives of the Research

This study focuses on studying the low-Mach number aerodynamic behaviour of the blended wing body aircraft at a 50 m/s and AOA ranging from $0^o$ to $40^o$. The L/D ratio has been observed at varying angles of attack to study the aerodynamic efficiency of the BWB. Several modifications such as adding winglets, changing the sweep angle, airfoils, aspect ratio, and wingspan are done on the baseline model in an attempt to decrease the drag, thus increasing the L/D ratio.

The main objectives of this study are presented in Table 2.

## 4.0 Methodology

### 4.1 Methodology Workflow (Figure 4)

### 4.2 Baseline Model

#### 4.2.1 Geometry

In this study, a blended wing body model has been designed, referring previous works by Naidu et al.[16] and Khan[14] in 2016 (Khan, 2016). Figure 5. presents the baseline BWB geometry designed for this study. This baseline model has been designed using the CAD software, Fusion 360. The engines and propulsion systems have been omitted from this baseline model to simplify the model for calculations. The dimensions of the model are shown in Figure 6. and the specifications of the inner and outer wings of the model are presented in Table.3.

The airfoils employed for the center body and outer wing are NACA 0012-64 (Figure 7) and NASA SC(2)-0710 (Figure 8) respectively.

The center body of the BWB or the fuselage requires a lower sectional lift coefficient when compared to the outboard wings. This allows for a thicker center body, thus maximizing the cabin space and payload capacity of the aircraft[17]. NACA 0012-64 airfoil has been used for the center body as it meets all of these conditions. For the outboard

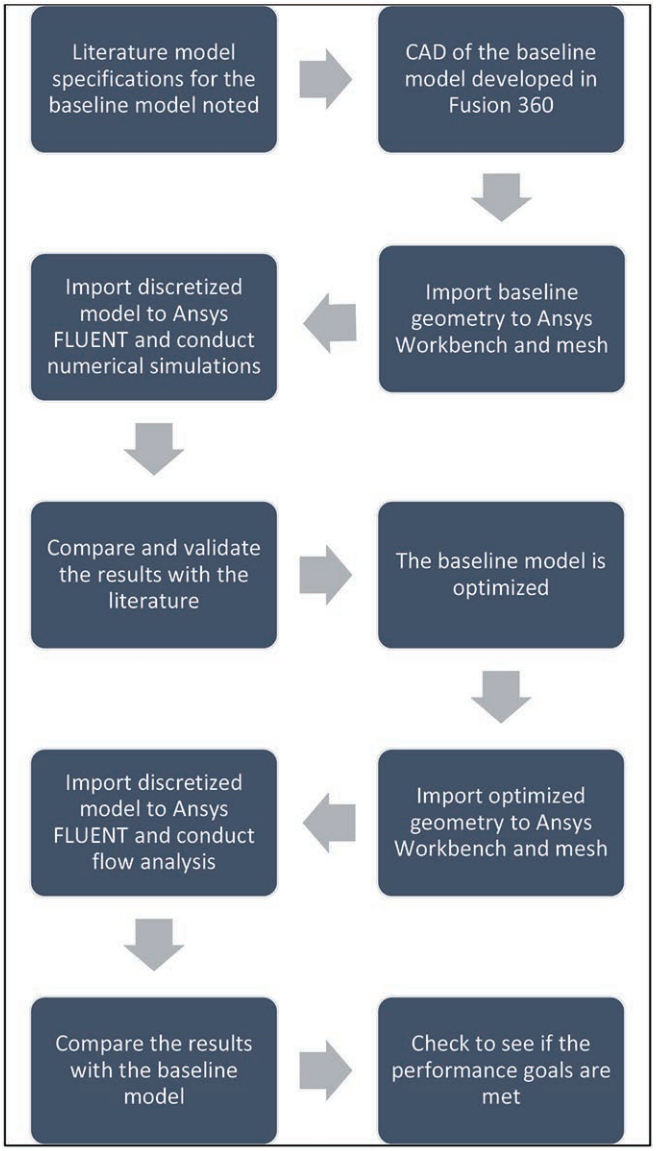


Figure 4: Methodology Workflow

**Table 2: Research Objectives**

| Objective No. | Aim |
|---|---|
| Objective I | Model, mesh, and obtain the flow analysis results for the baseline model of BWB |
| Objective II | Compare and validate the results of flow analysis on the baseline model with that of the literature results |
| Objective III | Modify the model by introducing winglets, changing airfoil shapes, and changing sweep angle |
| Objective IV | Compare the results of the modified model with the baseline model |

Figure 5: BWB Geometry - Baseline

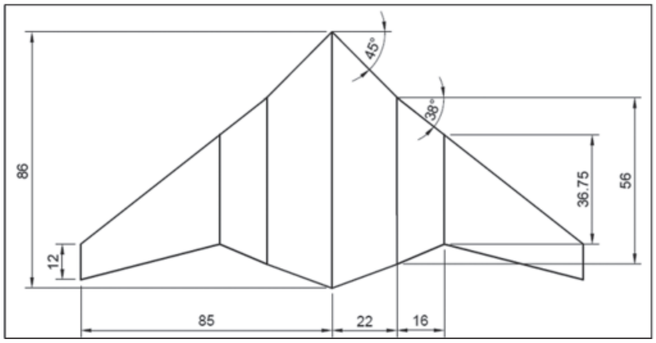


Figure 6: Dimensions of the Baseline Model (in mm)

**Table 3: Baseline Model Specifications**

| | Inner Wing | Outer Wing |
|---|---|---|
| Sweep Angle | 45° | 38° |
| Max Chord Length | 86 mm | 56 mm |
| Min Chord Length | 56 mm | 12 mm |
| Taper Ratio | 0.6512 | 0.214 |
| Airfoil used | NACA 0012-64 | NASA SC(2)-0710 |
| Wing Aspect Ratio | 0.3 | 1.78 |
| Wing Span | 22 mm | 63 mm |

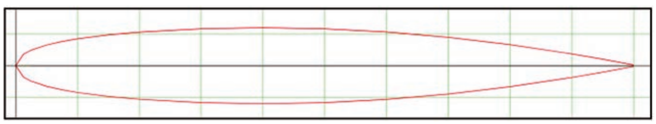

Figure 7: Center body cross-section (NACA 0012-64 (Naca001264-Il), n.d.)

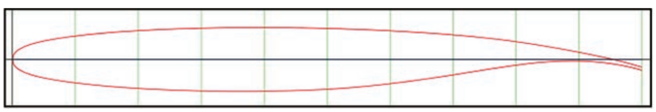

Figure 8: Outer wing cross-section (NASA SC(2)-0710 AIRFOIL (Sc20710-Il), n.d.)

wing, NASA SC(2)-0710, which is a supercritical airfoil, has been used to obtain higher lift coefficients and shock delaying characteristics.

The dimensions of the computational domain, created to conduct the flow analysis, are depicted in Table 4 and Figure 9 shows the model inside the enclosure which is used for the calculations. Symmetry has been used to reduce elements and hence the computational time.

**Table 4: Enclosure Specifications**

| Direction | Length |
|---|---|
| +X | 500 mm |
| +Y | 180 mm |
| +Z | 180 mm |
| -X | 300 mm |
| -Y | 180 mm |
| -Z | 180 mm |

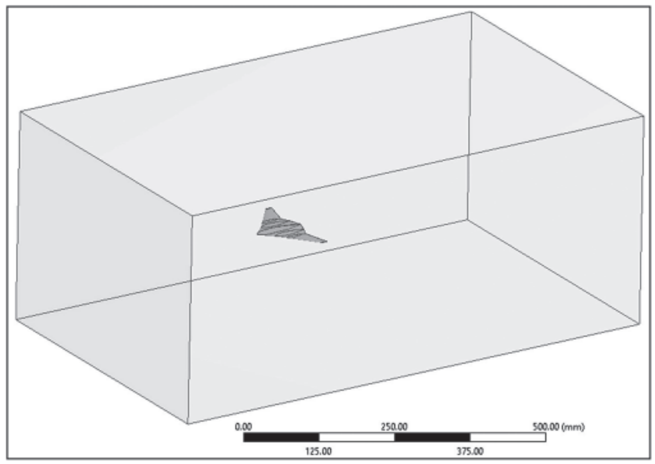


Figure 9: Baseline Model within the Computational Enclosure

### *4.2.2 Discretization*

Owing to the complexity of the model, an unstructured grid was used which also significantly reduced the meshing time. The grid used for the simulation is shown in the close-up top view and isometric view in Figure 10 (a) and (b) respectively. The mesh size, metrics, and statistics are presented in a tabulated form in Table 5. Before transferring to FLUENT, the different faces of the domain were named inlet, outlet, symmetry, wall, and aircraft.

## 4.3 Modified Model

### *4.3.1 Geometry*

Figure 11 presents the modified blended wing body model, designed on Fusion 360. Along with a few dimension

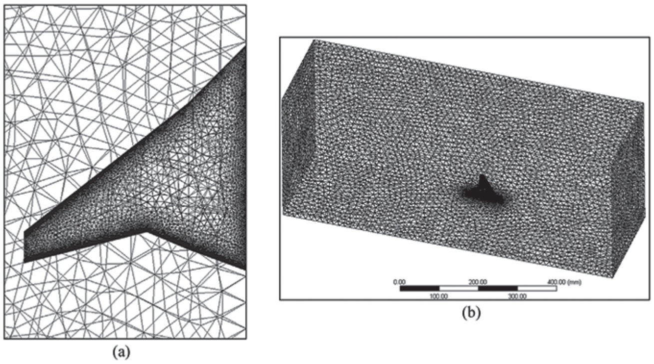


Figure 10: Mesh: (a) Top view; (b) Isometric view

**Table 5: Mesh Statistics and Metrics**

| | |
|---|---|
| Number of elements | 1799976 |
| Number of nodes | 322984 |
| Maximum skewness | 0.79819 |
| Average element quality | 0.83599 |
| Average aspect ratio | 1.8453 |

Figure 11: BWB Geometry – Modified

changes, winglets have been added to the model. Introducing winglets at the wingtips of an aircraft reduces the induced drag and also increases the lift to drag ratio[7]. Winglets tend to generate lift just like a wing, but in a perpendicular direction to the relative wind. This forward lift opposes the drag that is produced because of the wingtip vortices, thus reducing the overall induced drag. For this study, blended winglets are used. Since blended winglets do not produce interference drag, they reduce more drag as compared to the winglets that attach to the wing at about $90^{o}$[2]. The Airfoil used for the centerbody has been modified to NASA SC(2)-0518 (Figure 12), which is a supercritical airfoil. This will allow the centerbody to produce a higher lift than before, along with the wing, thus increasing the overall lift produced.

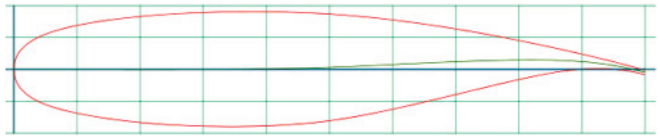

Figure 12: Center Body cross-section (NASA SC(2)-0518 AIRFOIL (Sc20518-Il), n.d.)

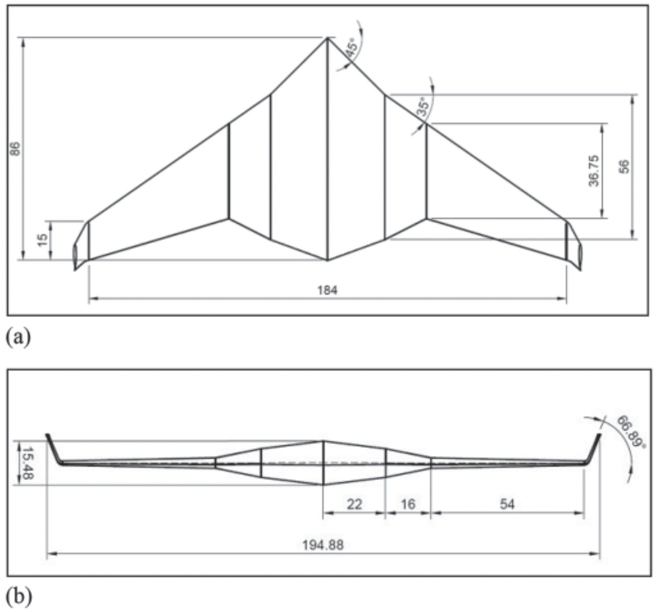


Figure 13: Dimensions of the modified BWB model (in mm) – (a) Front and (b) Top views

The sweep angle of the outboard wing has been reduced to 35º, and the wingspan has been increased to 70 mm.

Figure 13 shows the dimensions of the modified BWB model in front and top views, and Table 6 shows the specifications of the model.

The enclosure dimensions used for the modified model are the same as the baseline (Table 3). The modified model enclosed inside the computational enclosure has been depicted in Figure 14.

### *4.3.2 Discretization*

The grid used for the simulation is shown in the close-up top view and isometric view in Figure 15 (a) and (b) respectively. The mesh size, metrics, and statistics are presented in a tabulated form in Table 7. Before transferring to FLUENT, the faces of the computational domain were named inlet, symmetry, wall, outlet and aircraft.

## 4.4 Boundary Conditions and Set up

The boundary conditions and set up for both, the baseline and the modified model, have been kept the same. Velocity-inlet has been selected as the inlet boundary condition, with

**Table 6: Modified Model Specifications**

| | Inner Wing | Outer Wing |
|---|---|---|
| Sweep Angle | 45$^o$ | 35$^o$ |
| Max Chord Length | 86 mm | 56 mm |
| Min Chord Length | 56 mm | 15 mm |
| Taper Ratio | 0.6512 | 0.268 |
| Airfoil used | NASA SC(2)-0518 | NASA SC(2)-0710 |
| Wing Aspect Ratio | 0.3 | 1.78 |
| Wing Span | 22 mm | 70 mm |

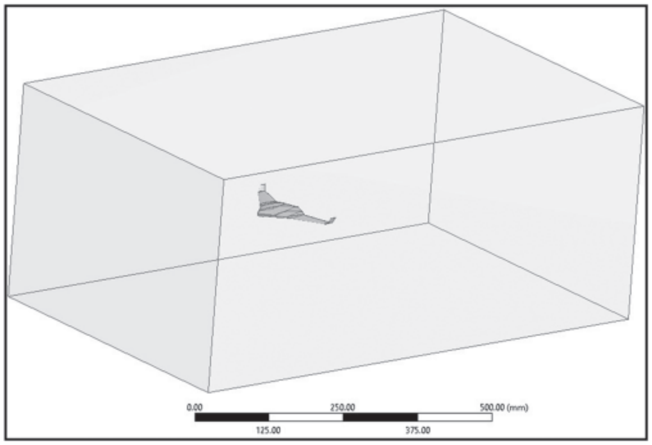


Figure 14: Modified Model within the Computational Enclosure

the inlet velocity set to 50 m/s. For outlet, pressure-outlet was taken as the boundary condition setting the gauge pressure as 0 Pa. A coupled solver is used for the calculations which solve the governing equations of continuity and momentum coupled together[30]. The two-equation RANS model, k-$\omega$ SST has been chosen as the turbulence model for this study. This turbulence model is known to provide more accuracy and a relatively better prediction for flow separation as compared to other models such as the Spalart Allmaras or the k-ε. The convergence monitors were set to 1e-06, and the simulations were run for 1500 iterations.

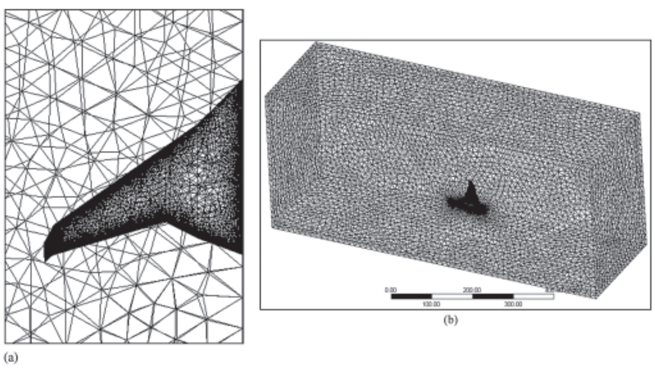


Figure 15: Mesh: (a) Top view; (b) Isometric view

**Table 7: Mesh Statistics and Metrics**

| | |
|---|---|
| Number of elements | 1926369 |
| Number of nodes | 345490 |
| Maximum skewness | 0.79867 |
| Average element quality | 0.83614 |
| Average aspect ratio | 1.8445 |

# 5.0 Results and Discussion

## 5.1 Baseline Results

The performance evaluation of the reference model in the literature is done using an inviscid model. The baseline model was initially simulated at a 0$^o$ angle of attack and 50 m/s velocity, using literature specifications in order to validate the results. Results for the validation are presented in Table 8.

**Table 8: Baseline results with an inviscid flow model**

| AoA | $C_L$ | $C_D$ | L/D |
|---|---|---|---|
| $\alpha$=0$^o$ | 0.014682027 | 0.43153979 | 29.39238499 |

The baseline BWB model was then simulated using the turbulence model k-*w* SST in Ansys FLUENT, for angles of attack 0$^o$, 10$^o$, 20$^o$, 30$^o$ and 40$^o$ at a low subsonic velocity of 50 m/s. Using a turbulence model provides a more practical solution, as it takes into account the viscosity of the flow, unlike the inviscid model which neglects the viscosity. Subsections 5.1.1 to 5.1.5 present the flow contours and results of the baseline flow simulation at all the five angles of attack.

### *5.1.1 Angle of Attack, $\alpha$=0$^o$*

Figure 16 depicts the aerodynamic behaviour of the flow around the BWB model at a velocity of 50 m/s. The Figure 16 (a) and (b) show the distribution of pressure on the top and bottom surfaces of the BWB. It was observed that the pressure on the bottom surface is higher than that of the top surface. This results in a total net force or lifts in the upward direction. Since the fuselage of the BWB is also shaped like an airfoil, it produces lift along with the wings of the BWB. This can be observed in Figure 16 (c) and (d), which shows the two-dimensional view of the center plane of the BWB. The pressure and velocity distribution can be observed through these figures.

The maximum and minimum values of pressure and velocity are tabulated in Table 9. The maximum pressure is experienced by the BWB at the leading edge, which can also be observed in Figure 16(c). At the center of the upper

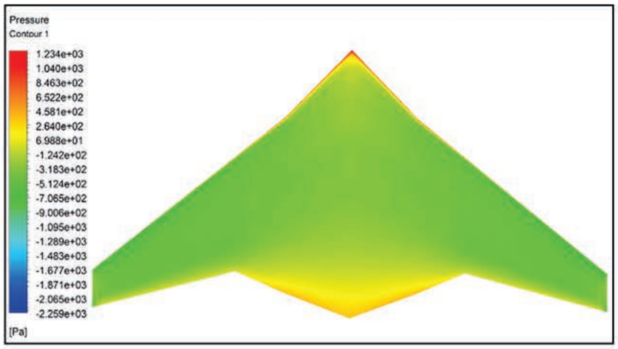


(a)

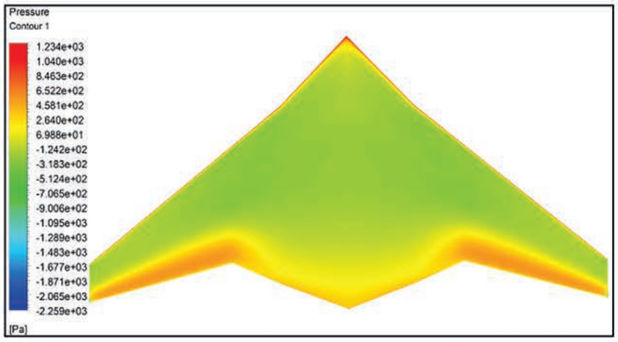


(b)

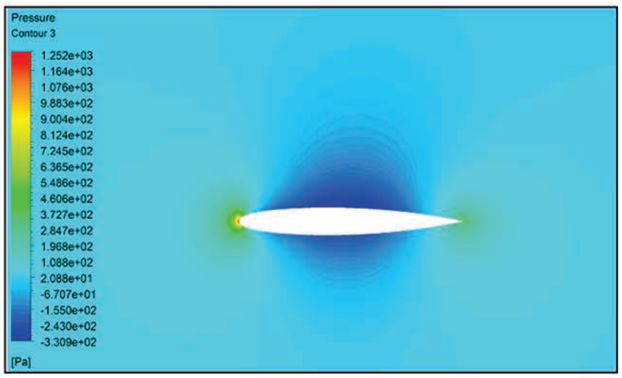


(c)

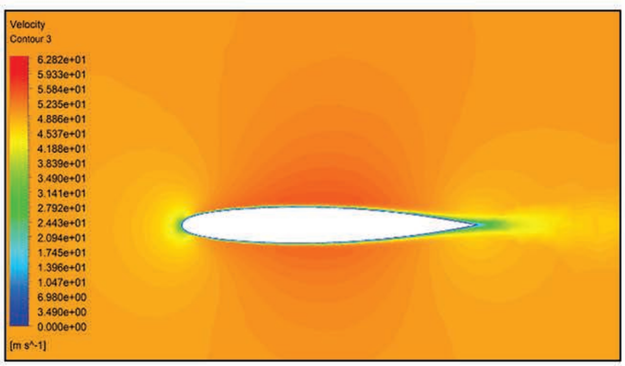


(d)

Figure 16: Flow contours - $\alpha$=0$^o$ – (a) Pressure: Upper surface, (b) Pressure: Lower surface, (c) Pressure: Side view, (d) Velocity

**Table 9: Minimum and Maximum Pressure and Velocity at $\alpha$=0$^o$**

| Max P (Pa) | Min P (Pa) | Max V (m/s) | Min V (m/s) |
|---|---|---|---|
| 1266.84 | -330.92 | 55.25272 | 40.31245 |

surface, the least amount of pressure is being exerted on the aircraft by the flow.

## *5.1.2 Angle of Attack, $\alpha$=10$^o$*

The flow contours of pressure and velocity at $\alpha$=10$^o$ are presented in Figure 16(a), (b) and (c). The pressure at the bottom surface of the BWB increases further, thus generating more lift as compared to 0$^o$. The drag also increases as a result of an increment in $\alpha$. Hence, the overall $C_L$ and $C_D$ increases, thus increasing the L/D.

Table 10 presents the maximum and minimum pressure and velocity experienced by the BWB. The point of highest pressure moves further towards the lower surface, and the lowest pressure point moves towards the leading edge. It can be observed that the flow velocity is higher on the top side of the BWB as a result of lower pressure.

**Table 10: Minimum and Maximum Pressure and Velocity at $\alpha$=10$^o$**

| Max P (Pa) | Min P (Pa) | Max V (m/s) | Min V (m/s) |
|---|---|---|---|
| 1338.37 | -814.958 | 60.8778 | 41.85557 |

## *5.1.3 Angle of Attack, $\alpha$=20$^o$*

Figure 18 (a), (b) and (c) depict the aerodynamic flow behaviour around the BWB at 50 m/s velocity and $\alpha$=20$^o$. A further increment of pressure and thus the lift can be observed.

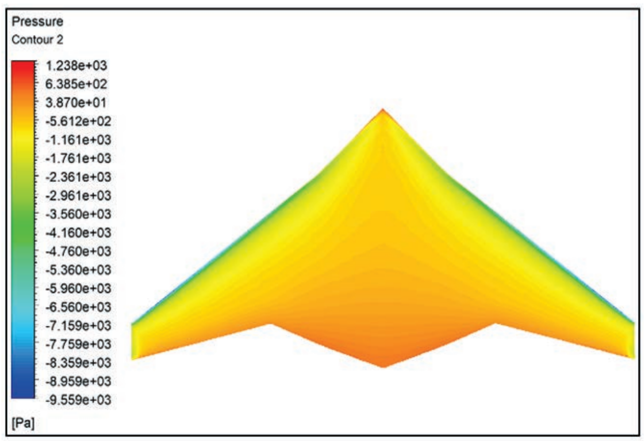


(a)

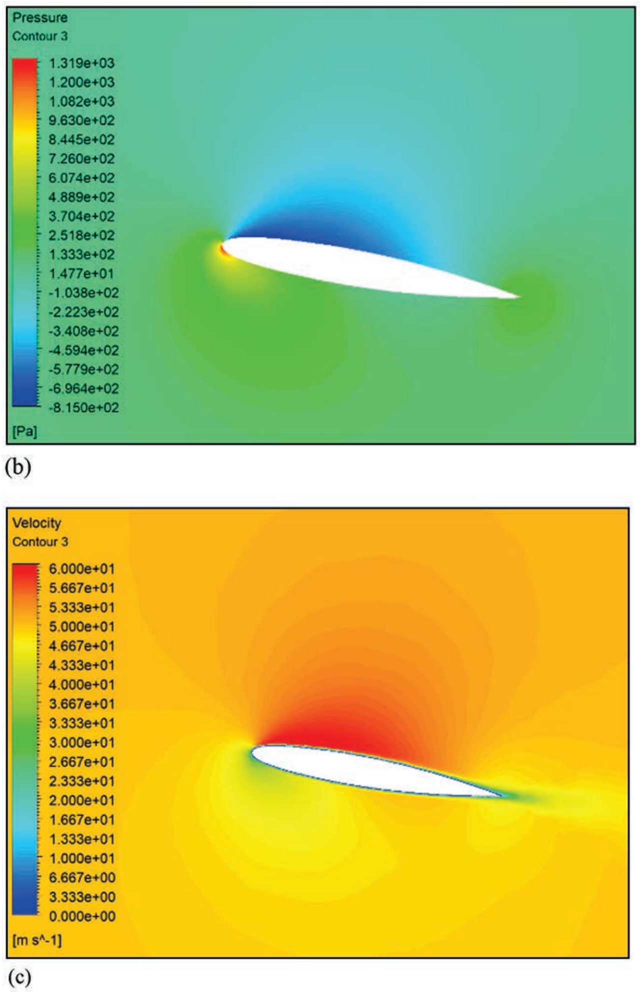


Figure 17: Flow contours - $\alpha$=10º – (a) Pressure: Upper surface, (b) Pressure: Side view, (c) Velocity

The minimum and maximum pressure and velocity for $\alpha=20^{o}$ have been tabulated in Table 11. An increment can be observed in the pressure as well as the velocity as the angle of attack increases.

### 5.1.4 Angle of Attack, $\alpha=30^{o}$

Figure 19 (a), (b) and (c) depict the aerodynamic flow behaviour around the BWB at 50 m/s velocity and $\alpha=30^{o}$.

The minimum and maximum pressure and velocity for $\alpha=30^{o}$ have been tabulated in Table 12.

### 5.1.5 Angle of Attack, $\alpha=40^{o}$

Figure 20 (a), (b) and (c) depict the aerodynamic flow behaviour around the BWB at 50 m/s velocity and $\alpha=40^{o}$. It can be observed through the velocity contour, i.e., Figure 20(c), that the flow velocity at the trailing edge of the aircraft model decreases and vortices start to form in this wake region, as the flow starts to separate. This happens because

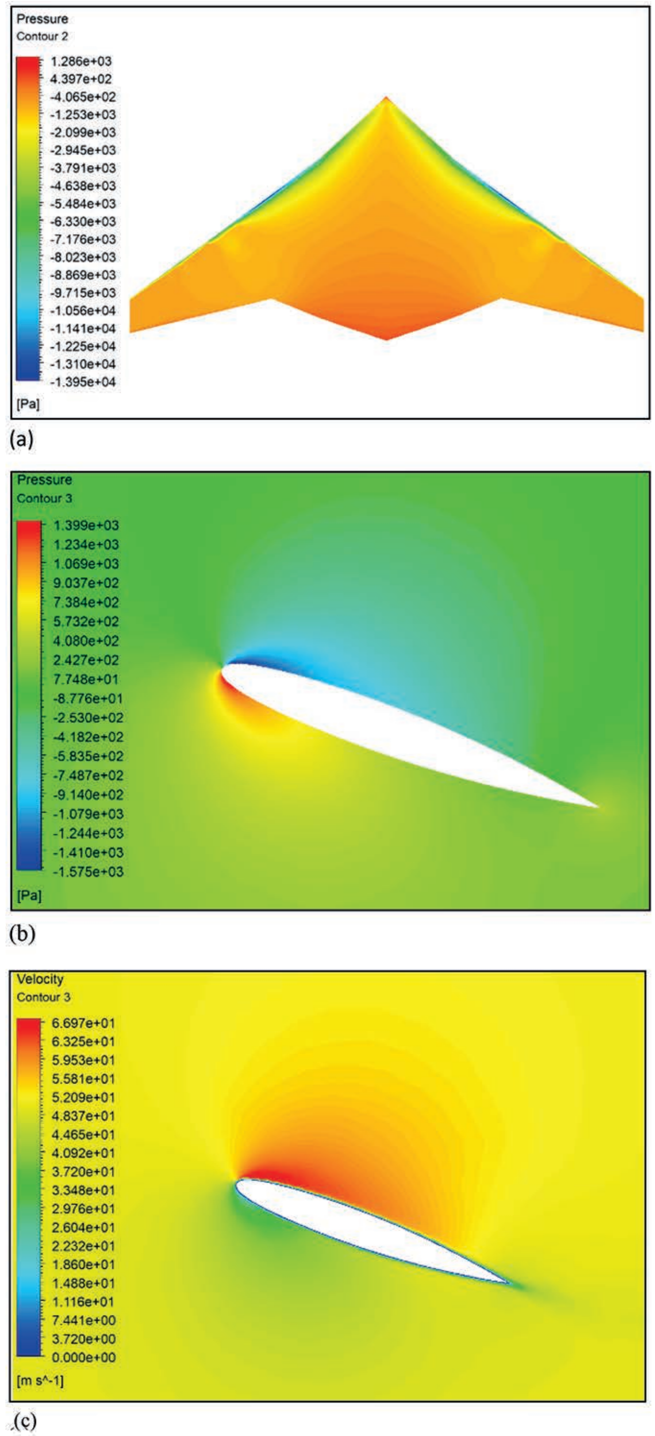


Figure 18: Flow contours $\alpha$=20º – (a) Pressure: Upper surface, (b) Pressure: Side view, (c) Velocity

the model has now reached past the point of maximum lift and as a result, the lift will go on decreasing if there is any further increase in the angle. It is known as the stall condition. It can, however, be observed that the BWB can produce lift at higher AOAs and even at the stall, unlike the

**Table 11: Minimum and Maximum Pressure and Velocity at $\alpha$=20$^{o}$**

| Max P (Pa) | Min P (Pa) | Max V (m/s) | Min V (m/s) |
|---|---|---|---|
| 1462.94 | -1574.93 | 68.96214 | 41.97923 |

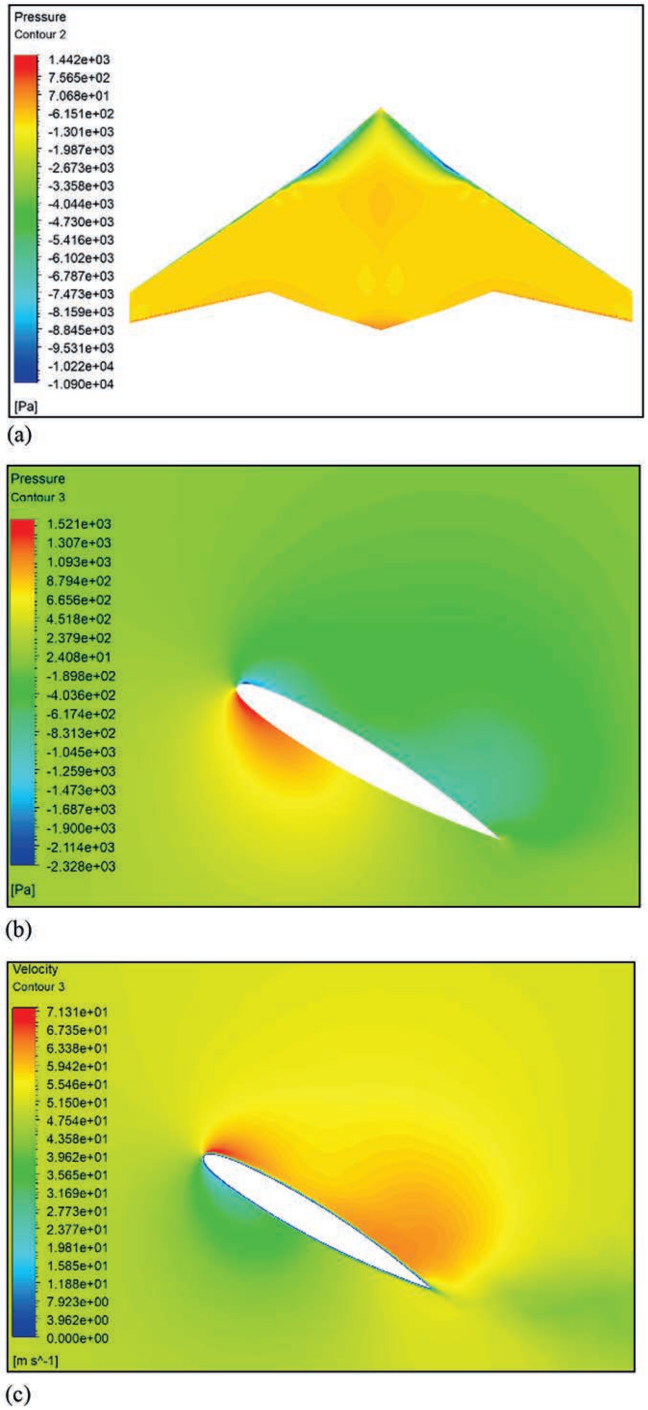


Figure 19: Flow contours - $\alpha$=30$^{o}$ – (a) Pressure: Upper surface, (b) Pressure: Side view, (c) Velocity

**Table 12: Minimum and Maximum Pressure and Velocity at $\alpha$=30$^{o}$**

| Max P (Pa) | Min P (Pa) | Max V (m/s) | Min V (m/s) |
|---|---|---|---|
| 1556.61 | -2328.16 | 75.50807 | 42.08673 |

conventional aircraft which is unable to generate any lift at this point and the altitude starts to reduce as a result. A sudden drop can also be observed in the L/D ratio (Table 14).

The minimum and maximum pressure and velocity are presented in Table 13. Here, the point having the minimum velocity is observed to shift towards the end of the model as a result of the stall. The maximum pressure at the bottom of the aircraft increases, but pressure also increases on the upper surface, thus generating less lift.

The results of lift and drag coefficients of the baseline analysis are presented in Table 14 and a plot of lift to drag ratio vs $\alpha$ is depicted in Figure 21. $C_L$ increases along with the angle of attack up to 20$^{o}$, and starts to decrease after that. Likewise, the L/D ratio rises with $\alpha$ up to 20$^{o}$. The maximum L/D ratio of 44.81 has been observed at $\alpha$=20$^{o}$. It

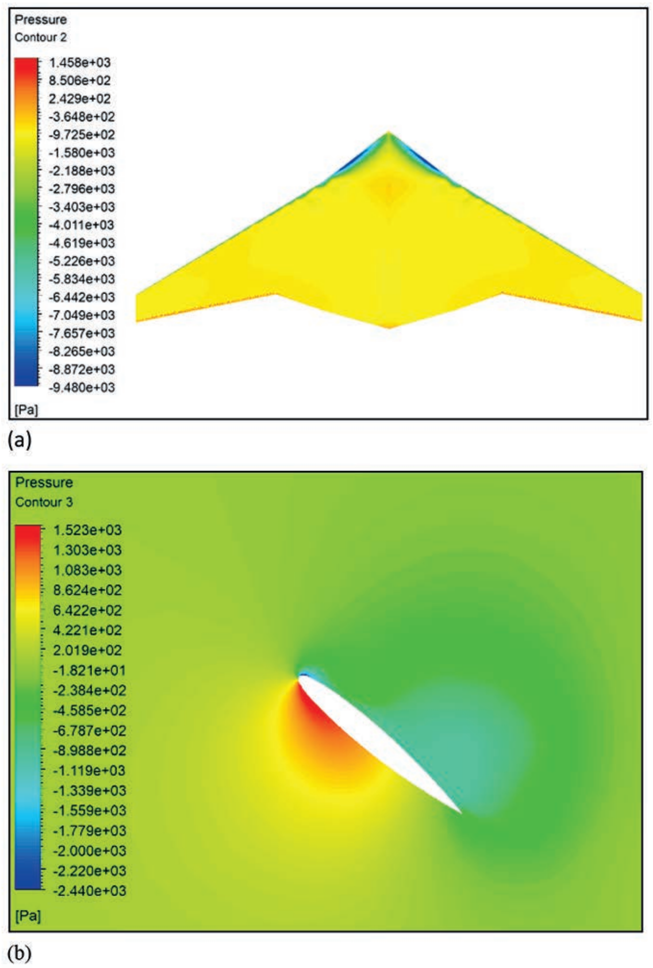

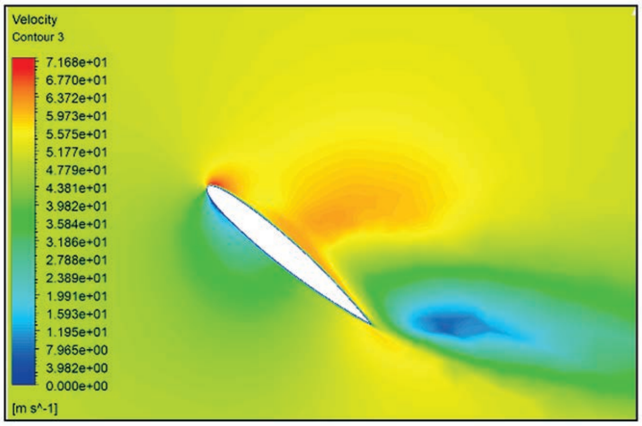


(c)

Figure 20: Flow contours - $\alpha$=40$^{o}$ – (a) Pressure: Upper surface, (b) Pressure: Side view, (c) Velocity

starts to decrease after this point, and a sudden drop can be observed at 40$^{o}$, where the aircraft stalls.

## 5.2 Modified Results

### 5.2.1 Angle of Attack, $\alpha$=0$^{o}$

The flow contours of pressure and velocity for the modified model at 0$^{o}$ angle of attack have been presented in Figure 22 (a), (b) and (c). Here a supercritical airfoil has been used for both the centerbody and outer wing of the BWB. Research on supercritical airfoils indicates that they can produce high lift coefficients and aid in the delay of flow separation. Comparatively higher pressure on the bottom surface and lower pressure on the top surface can be observed for the model. The pressure is decreasing from the nose of the BWB to the wing tips.

**Table 13: Minimum and Maximum Pressure and Velocity at $\alpha$=40$^{o}$**

| Max P (Pa) | Min P (Pa) | Max V (m/s) | Min V (m/s) |
|---|---|---|---|
| 1568.91 | -2439.85 | 77.23173 | 39.33523 |

**Table 14: Baseline Results**

| AoA | Velocity | $C_D$ | $C_L$ | L/D |
|---|---|---|---|---|
| $\alpha$=0$^{o}$ | 50m/s | 0.0153 | 0.328 | 21.397 |
| $\alpha$=10$^{o}$ | 50m/s | 0.0162 | 0.567 | 34.834 |
| $\alpha$=20$^{o}$ | 50m/s | 0.0163 | 0.732 | 44.809 |
| $\alpha$=30$^{o}$ | 50m/s | 0.0169 | 0.680 | 40.151 |
| $\alpha$=40$^{o}$ | 50m/s | 0.0248 | 0.646 | 25.963 |

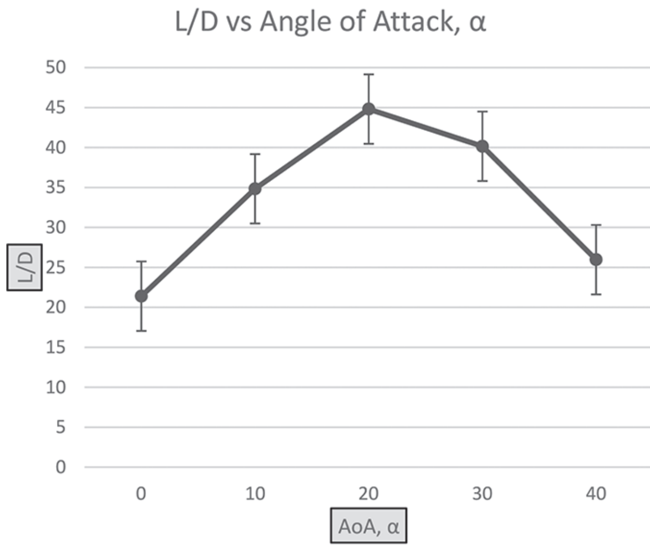


Figure 21: The plot of L/D vs Angle of attack for the baseline model

Table 15 presents the minimum and maximum values of pressure and velocity for the modified model at a 0$^{o}$ angle of attack. The maximum pressure can be observed at the leading-edge tip or nose of the BWB. Minimum pressure is being exerted on the upper surface of the BWB by the airflow.

The velocity vectors around the winglet of the modified BWB model are shown in Figure 23. The winglets increase the cruising range along with the fuel efficiency of the aircraft (NASA, 2004). The unequal pressure that is essential for the generation of lift by the aircraft wings causes the air on the lower surface to flow in the outward direction along with the wingtips which then move inwards along the upper side of the wing. This gives rise to wingtip vortices, which increase the drag while decreasing the overall lift produced. The winglets, however, produce a forward thrust which reduces the strength of these vortices, thus reducing the drag generated by them. Winglets are more effective at high angles of attack.

### 5.2.2 Angle of Attack, $\alpha$=10$^{o}$

Figure 24 (a), (b) and (c) depict the aerodynamic flow behaviour around the modified BWB at 50 m/s velocity and $\alpha$=10$^{o}$.

The minimum and maximum pressure and velocity for $\alpha$=10$^{o}$ have been tabulated in Table 16.

**Table 15: Minimum and Maximum Pressure and Velocity at $\alpha$=0$^{o}$**

| Max P (Pa) | Min P (Pa) | Max V (m/s) | Min V (m/s) |
|---|---|---|---|
| 1365.49 | -535.419 | 57.92 | 39.13 |

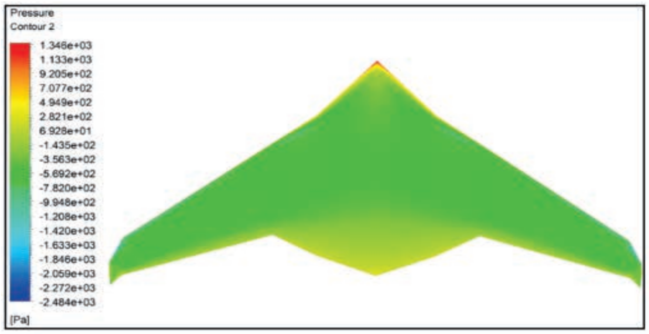


(a)

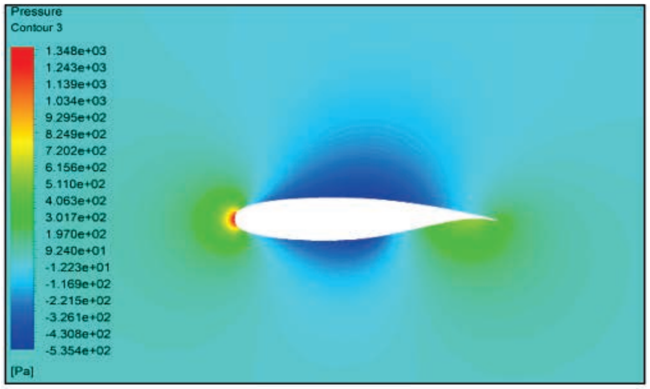


(b)

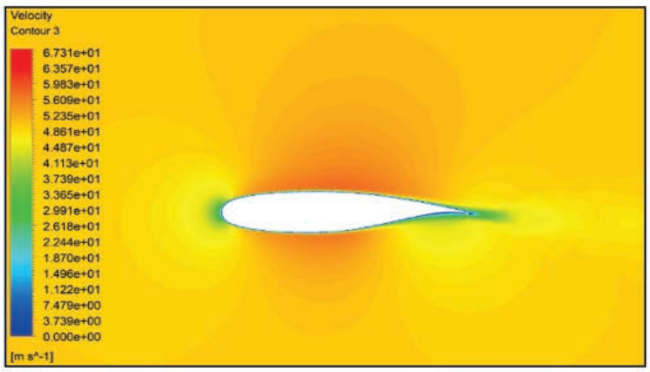


(c)

Figure 22: Flow contours - $\alpha$=0$^{o}$ – (a) Pressure: Upper surface, (b) Pressure: Side view, (c) Velocity

### 5.2.3 Angle of Attack, $\alpha$=20$^{o}$

Figure 25 (a), (b), and (c) depict the aerodynamic flow behaviour around the modified BWB at 50 m/s velocity and $\alpha$=20$^{o}$.

The minimum and maximum pressure and velocity for $\alpha$=20$^{o}$ have been tabulated in Table 17.

### 5.2.4 Angle of Attack, $\alpha$=30$^{o}$

Figure 26 (a), (b) and (c) depict the aerodynamic flow behaviour around the modified BWB at 50 m/s velocity and $\alpha$=30$^{o}$.

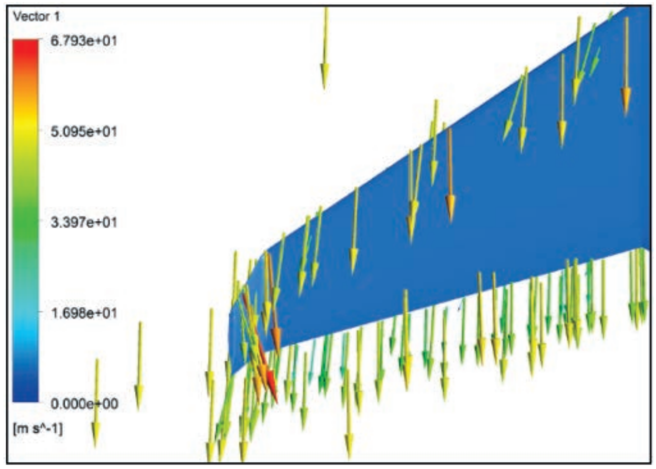


Figure 23: Velocity Vectors around the Winglet

The minimum and maximum pressure and velocity for $\alpha$=30$^{o}$ have been tabulated in Table 18.

### 5.2.5 Angle of Attack, $\alpha$=40$^{o}$

The aerodynamic flow behaviour of the modified BWB model has been depicted in Figure 27 (a), (b) and (c). The modified model also stalls at $\alpha$=40$^{o}$. When compared to the

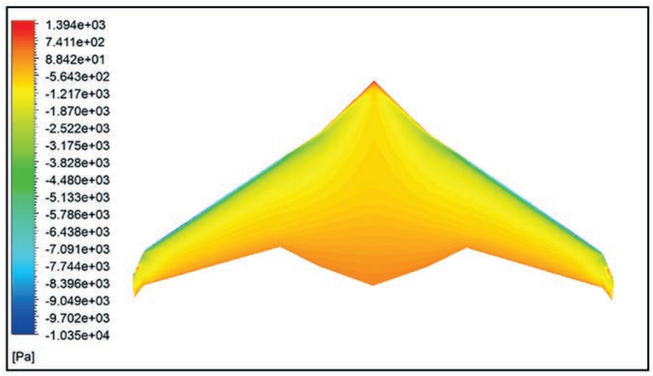


(a)

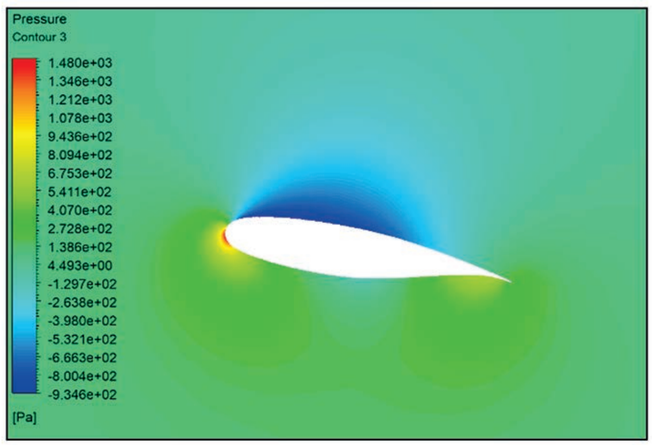


(b)

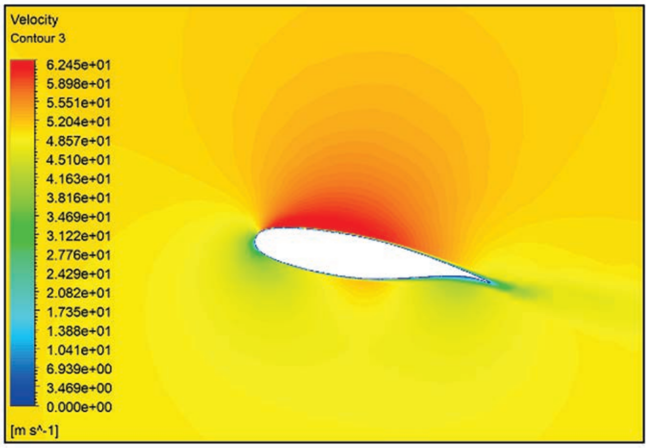


(c)

Figure 24: Flow contours - $\alpha$=10$^{o}$ – (a) Pressure: Upper surface, (b) Pressure: Side view, (c) Velocity

**Table 16: Minimum and Maximum Pressure and Velocity at $\alpha$=10$^{O}$**

| Max P (Pa) | Min P (Pa) | Max V (m/s) | Min V (m/s) |
|---|---|---|---|
| 1502.55 | -934.59 | 63.2 | 36.51 |

**Table 17: Minimum and Maximum Pressure and Velocity at $\alpha$=20$^{o}$**

| Max P (Pa) | Min P (Pa) | Max V (m/s) | Min V (m/s) |
|---|---|---|---|
| 1522.288 | -1526.15 | 69.67 | 37.65 |

**Table 18: Minimum and Maximum Pressure and Velocity at $\alpha$=30$^{o}$**

| Max P (Pa) | Min P (Pa) | Max V (m/s) | Min V (m/s) |
|---|---|---|---|
| 1555.98 | -1941 | 74.3 | 38.33 |

baseline, the lift generated is higher for the modified model. The flow separation can be observed in Figure 27(c).

The minimum and maximum pressure and velocity for $\alpha$=40$^{o}$ have been tabulated in Table 19.

The results of lift and drag coefficients for the modified analysis are presented in Table 20., and a plot of lift to drag ratio vs angle of attack is depicted in Figure 28. $C_L$ increases along with the angle of attack up to 30$^{o}$, and starts to decrease after that. Likewise, the L/D ratio increases with $\alpha$ up to 30$^{o}$. The maximum L/D ratio of 44.31 has been observed at $\alpha$=30$^{o}$. It starts to decrease after this point, and a sudden drop can be observed at 40$^{o}$, where the aircraft stalls.

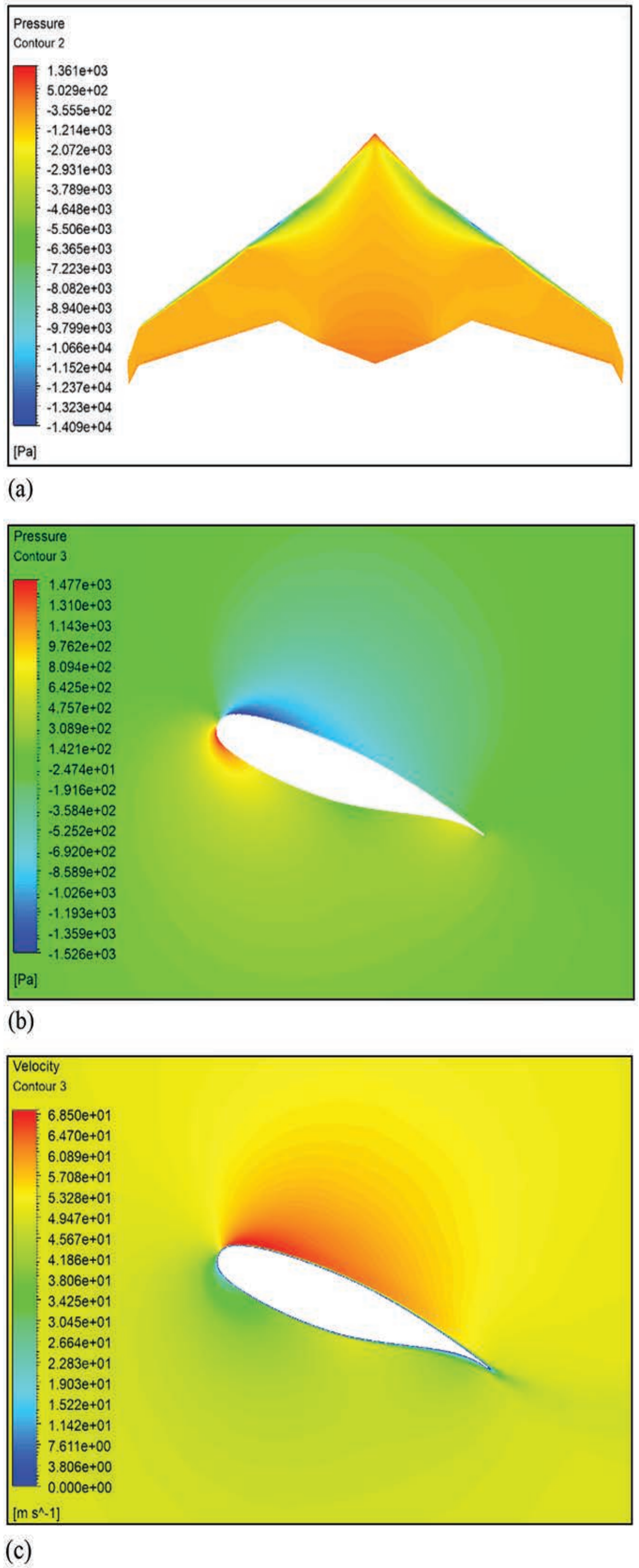


Figure 25: Flow contours - $\alpha$=20$^{o}$ – (a) Pressure: Upper surface, (b) Pressure: Side view, (c) Velocity

## 5.3 Validation

The results of the baseline analysis were found to be consistent with the reference literature[16]. The slight difference in the results could be because of a few assumed dimensions for the baseline model. Table 21 presents the results of the reference model, baseline model, and the modified model at an angle of attack of $0^{o}$.

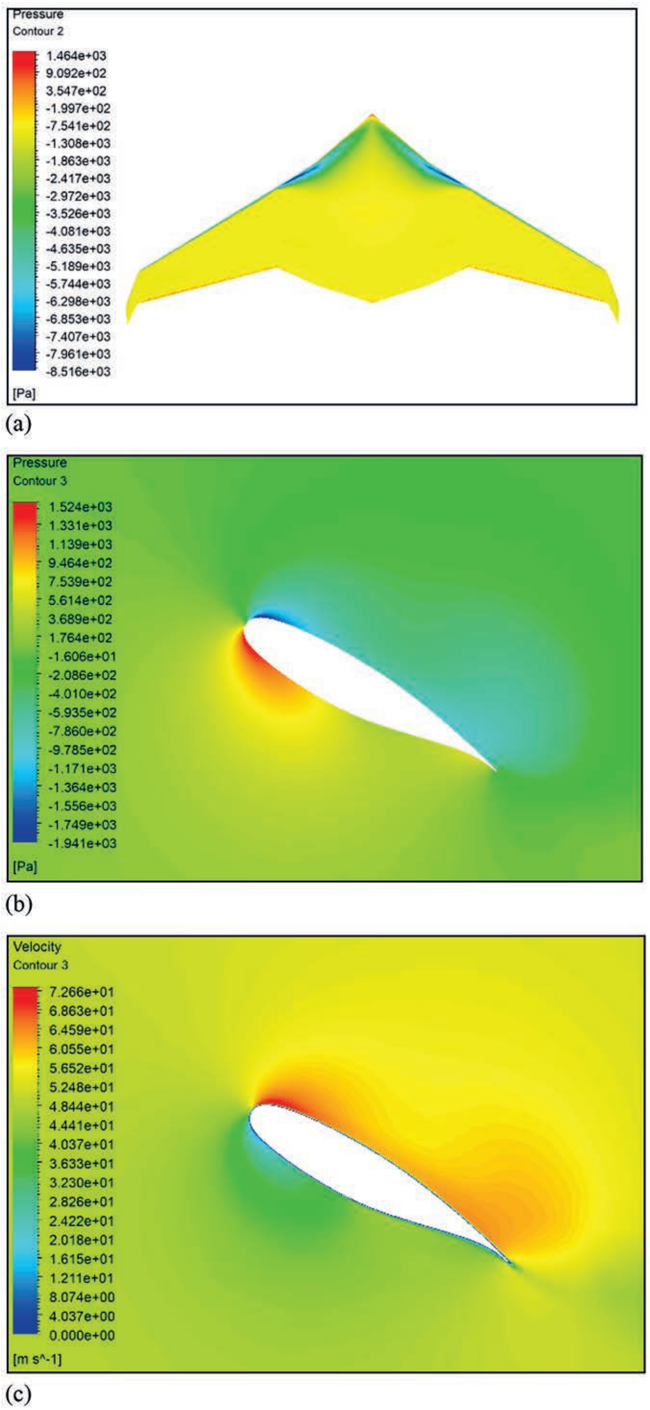


Figure 26: Flow contours - $\alpha=30^{o}$ – (a) Pressure: Upper surface, (b) Pressure: Side view, (c) Velocity

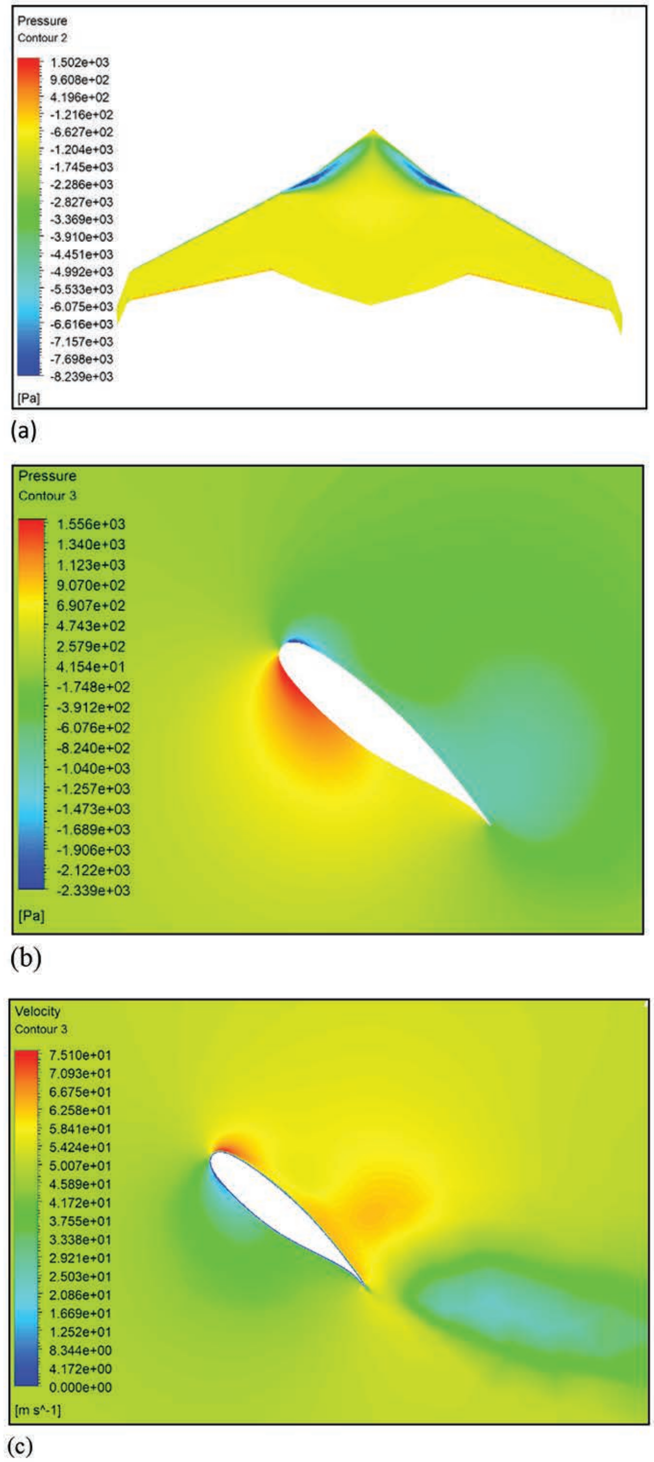


Figure 27: Flow contours - $\alpha=40^{o}$ – (a) Pressure: Upper surface, (b) Pressure: Side view, (c) Velocity

**Table 19: Minimum and Maximum Pressure and Velocity at $\alpha$=40$^o$**

| Max P (Pa) | Min P (Pa) | Max V (m/s) | Min V (m/s) |
|---|---|---|---|
| 1592.21 | -2338.56 | 77.61 | 38.81 |

**Table 20: Modified Results**

| Angle of Attack | Velocity (m/s) | $C_L$ | $C_D$ | L/D |
|---|---|---|---|---|
| $\alpha$=0$^o$ | 50 | 0.667 | 0.019 | 35.104 |
| $\alpha$=10$^o$ | 50 | 0.7 | 0.021 | 32.944 |
| $\alpha$=20$^o$ | 50 | 0.772 | 0.019 | 40.569 |
| $\alpha$=30$^o$ | 50 | 0.761 | 0.0171 | 44.317 |
| $\alpha$=40$^o$ | 50 | 0.761 | 0.024 | 30.623 |

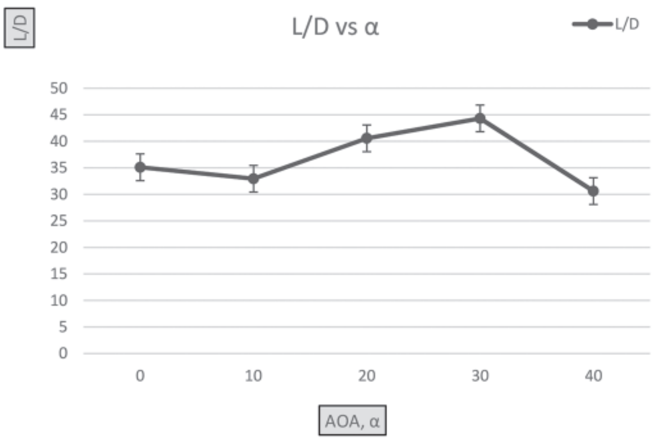


Figure 28: The plot of L/D vs AOA for modified results

## 6.0 Conclusions

The blended wing body aircraft configuration was conceptualized about 35 years ago, to meet the future demands of air transportation: noise reduction, fuel efficiency, etc., which could not be met by the conventional TAW aircraft. The concept was found to be superior to the conventional design in numerous ways. Researchers explored this concept further other the past few years extensively, in an attempt to study the configuration and make it feasible for air transportation.

This paper mainly aims to study the aerodynamic behaviour of a BWB aircraft through CFD analysis. A baseline BWB model has been designed based on the reference model. The aerodynamic performance of this model has been analyzed at different angles of attack ranging from 0$^o$ to 40$^o$, where the lift to drag ratio for 0$^o$ is found to be 33.19. The validation of these results with the literature suggests similarity in the performance of the baseline model. A new model, with several modifications: addition of winglets; change in sweep angle, airfoil, and aspect ratio, was then designed and simulated at angles 0$^o$, 10$^o$, 20$^o$, 30$^o$ and 40$^o$. The effects of winglets in drag reduction have also been discussed and demonstrated in Figure 23. Using a supercritical airfoil for the centerbody of the BWB allows the fuselage to produce a larger amount of lift as compared to the one used for the baseline. A significant improvement of around 19% is observed for the modified model at a 0$^o$ angle of attack. According to the literature, a 20% improvement in the L/D ratio was conceptualized for a BWB configuration over the conventional design. A Boeing 747 and Lockheed U-2 have an L/D ratio of 17.7 and 25.6 respectively. Comparing this with the baseline and the modified model of this study, the improvement in the L/D is observed to be in satisfaction with the literature results.

**Table 21: Result Validation (Khan, 2016)**

| Aircraft | L/D Ratio |
|---|---|
| Reference Model | 33.85 |
| Designed BWB (Baseline) | 29.4 |
| Designed BWB (Modified) | 35.104 |

## 7.0 References


1. Airbus. (2020): Airbus reveals its blended wing aircraft demonstrator. https://www.airbus.com/en/newsroom/press-releases/2020-02-airbus-reveals-its-blended-wing-aircraft-demonstrator
2. Aleks Udris. (2016): https://www.boldmethod.com/learn-to-fly/aerodynamics/how-winglets-reduce-drag-and-how-wingtip-vortices-form/. http://www.boldmethod.com/learn-to-fly/aerodynamics/winglets-and-wingtip-vortices/
3. Ali, Z. M., Kuntjoro, W., Wisnoe, W., & Nasir, R. E. M. (2012): The effect of canard on aerodynamics of Blended Wing Body. *Applied Mechanics and Materials*, 110–116 (December 2015), 4156–4160. https://doi.org/10.4028/www.scientific.net/AMM.110-116.4156
4. Ali, Z.M., Kuntjoro, W., Wisnoe, W., Nasir, R.E.M., Mohamad, F. and Reduan, N.F. (2011): The aerodynamics performance of Blended Wing Body Baseline-II E2. 2011 IEEE 3rd International Conference on Communication Software and Networks, ICCSN 2011, December 2015, 293–297. https://doi.org/10.1109/ICCSN.2011.6014899
5. Angelo, S., Potty, V., Rao, P. S., & Srinivas, G. (2019):

Aircraft Fuselage Recent Developments - A Review. 7, 12–20. https://doi.org/10.13189/ujme.2019.071

6. Arokkiaswamy, A. and Nishanth P. (2020): Shape Investigation and Optimization of a Blended-Wing-Body Configuration using Wind Tunnel Simulation and Genetic Algorithm. Technology, Engineering and Management-A VTU Publication, 2(1), 18–26.
7. Bojja, A. and Garre, P. (2013): Analysis on Reducing the Induced Drag Using the Winglet at the Wingtip. *International Journal of Engineering Research & Technology*, 2(12), 51–53.
8. Brown, M. and Vos, R. (2018): Conceptual design and evaluation of blended-wing-body aircraft. AIAA Aerospace Sciences Meeting, 2018, 210059. https://doi.org/10.2514/6.2018-0522
9. Chen, Z., Zhang, M., Chen, Y., Sang, W., Tan, Z., LI, D. and Zhang, B. (2019): Assessment on critical technologies for conceptual design of blended-wing-body civil aircraft. *Chinese Journal of Aeronautics*, 32(8), 1797–1827. https://doi.org/10.1016/j.cja.2019.06.006
10. G, S. and Sanyam Handa. (2022): Recent developments of blended wing body aircraft/ : experimental, numerical and theoretical approaches. Aerospace Systems. https://doi.org/10.1007/s42401-022-00133-1
11. Ghigliazza, H. H., Martínez-Val, R., Perez, E. and Smrcek, L. (2007): Wake of transport flying wings. *Journal of Aircraft*, 44(2), 558–562. https://doi.org/10.2514/1.24298
12. Google. (n.d.).
13. Hill, G. A. and Thomas, R. H. (2004): Challenges and Opportunities for Noise Reduction Through Advanced Aircraft Propulsion Airframe Integration and Configurations. In 8th CEAS Workshop: Aeroacoustics of New Aircraft and Engine Configurations (pp. 1–13).
14. Khan, M.A.A.J. (2016): Computational Aerodynamic Analysis of Blended Wing Body Mav Design. *International Journal of Research in Engineering and Technology*, 05(11), 273–284. https://doi.org/10.15623/ijret.2016.0511045
15. Liebeck, R. H. (2003): Blended Wing Body design challenges. AIAA\ICAS International Air and Space Symposium and Exposition: The Next 100 Years, July, 1–12. https://doi.org/10.2514/6.2003-2659
16. Liebeck, R.H. (2004): Design of the Blended Wing Body Subsonic Transport. *Journal of Aircraft*, 41(1), 10–25. https://doi.org/10.2514/1.9084
17. Liebeck, R.H., Page, M.A. and Rawdon, B. K. (1998a): AIAA 98-0438 Blended-Wing-Body Subsonic Commercial Transport 36th Aerospace Sciences Meeting & Exhibit January 12-15 , 1998 / Reno , NV.
18. Liebeck, R.H., Page, M.A. and Rawdon, B. K. (1998b): Blended-Wing-Body subsonic commercial transport. 36th AIAA Aerospace Sciences Meeting and Exhibit. https://doi.org/10.2514/6.1998-438
19. Lyu, Z. and Martins, J.R.R.A. (2014): Aerodynamic design optimization studies of a blended-wing-body aircraft. *Journal of Aircraft*, 51(5), 1604–1617. https://doi.org/10.2514/1.C032491
20. Mahamuni, P., Kulkarni, A. and Parikh, Y. (2014): Aerodynamic study of blended wing body. *International Journal of Applied Engineering Research*, 9(24), 29247–29255.
21. Marino, M. and Sabatini, R. (2015): Benefits of the Blended Wing Body Aircraft Compared to Current Airliners. International Symposium on Sustainable Aviation (ISSA 2015), June.
22. Martinez-Val, R. (2020): Flying Wings . A New Paradigm for Civil Aviation/ ? Acta Polytechnica Vol. 47 No. 1/2007, 47(1). https://doi.org/https://doi.org/10.14311/914
23. Martínez-Val, R., Pérez, E., Alfaro, P. and Pérez, J. (2007): Conceptual design of a medium size flying wing. Proceedings of the Institution of Mechanical Engineers, Part G: *Journal of Aerospace Engineering*, 221(1), 57–66. https://doi.org/10.1243/09544100JAERO90
24. Martínez-Val, Rodrigo, Cuerno, C., Pérez, E., & Ghigliazza, H. H. (2010): Potential effects of blended wing bodies on the air transportation system. Journal of Aircraft, 47(5), 1599–1604. https://doi.org/10.2514/1.C000214
25. Martinez, R. M. (2014): Design and Analysis of the Control and Stability of a Blended Wing Body Aircraft. Royal Institute of Technology (KTH) Stockholm, Sweden, May, 1–167.
26. Melvin Philip, Venkatesh Kusnur, & Prashant Manvi. (2015): Design Optimization of a Ducted Fan Blended Wing Body UAV using CFD Analysis. *International Journal of Engineering Research* and, V4(09), 158–164. https://doi.org/10.17577/ijertv4is090214
27. Mohamad, F., Wisnoe, W., Kuntjoro, W., Nasir, R.E. M., Mohd. Ali, Z. and Reduan, N.F. (2010): Wind Tunnel experiments of UiTM's blended wing body (BWB) Baseline-II unmanned aerial vehicle (UAV) at low subsonic speed. CSSR 2010-2010 International Conference on Science and Social Research, December 2015, 991–994. https://doi.org/10.1109/CSSR.2010.5773934
28. Mv, M., Mondal, P., Karn, P. K. and Kumar, P. (2019): Numerical and Experimental Investigation of Blended Wing Body Configuration. 1–10.
29. NACA 0012-64 (naca001264-il). (n.d.). http://

airfoiltools.com/airfoil/details?airfoil=naca001264-il

30. Naidu, K. S., Keerthi, G.S. and Nikhil Bharadwaj, V.V.S. (2016): CFD Analysis of Blended Wing Body and B2 Wing. *International Journal of Engineering Sciences & Research Technology*, 5(2), 492–513.
31. NASA. (2004). Winglets. 1–4.
32. NASA SC(2)-0518 AIRFOIL (sc20518-il). (n.d.).
33. NASA SC(2)-0710 AIRFOIL (sc20710-il). (n.d.).
34. Okonkwo, P. and Smith, H. (2016): Review of evolving trends in blended wing body aircraft design. Progress in Aerospace Sciences, 82(April 2018), 1–23. https://doi.org/10.1016/j.paerosci.2015.12.002
35. Ordoukhanian, E. and Madni, A.M. (2014): Blended wing body architecting and design: Current status and future prospects. Procedia Computer Science, 28(Cser), 619–625. https://doi.org/10.1016/j.procs.2014.03.075
36. Peigin, S. and Epstein, B. (2006): Computational fluid dynamics driven optimization of blended wing body aircraft. *AIAA Journal*, 44(11), 2736–2745. https://doi.org/10.2514/1.19757
37. Potsdam, M.A., Page, M.A. and Liebeck, R.H. (1997): Blended Wing Body Analysis and Design. American Institute of Aeronautics and Astronautics, Inc.
38. Potty, V., Angelo, S., Rao, P.S. and Srinivas, G. (2019): Recent Developments of an Aircraft Fuselage along Theoretical, *Experimental and Numerical Approach - A Review*. 7, 21–28. https://doi.org/10.13189/ujme.2019.071403
39. Qin, N., Vavalle, A., Le Moigne, A., Laban, M., Hackett, K. and Weinerfelt, P. (2004): Aerodynamic considerations of blended wing body aircraft. Progress in Aerospace Sciences, 40(6), 321–343. https://doi.org/10.1016/j.paerosci.2004.08.001
40. Salazar-Jimenes, G., Lopez-Aguilar, H. A., Gomez, J. A., Chazao-Zaharias, A., Duerte-Moller, A. and Perez-Hernandez, A. (2018): Blended Wing CFD Analysis/: Aerodynamic. *International Journal of Mathematics and Computers in Simulation*, 12(September), 33–43.
41. Sharma, A., Alva, T. and Srinivas, G. (2015): Flow Analysis of Blended Wing Body (BWB) Using CFD Technique. 2(7), 555–559.
42. Thompson, D., Feys, J., Filewich, M., Abdel-Magid, S., Dalli, D. and Goto, F. (2011): The Design and Construction of a Blended Wing Body UAV. January, 1–11. https://doi.org/10.2514/6.2011-841
43. Valiyff, A. and Arjomandi, M. (2009): An investigation into the aerodynamic efficiency of tailless aircraft. 47th AIAA Aerospace Sciences Meeting Including the New Horizons Forum and Aerospace Exposition, January, 1–9. https://doi.org/10.2514/6.2009-1436
44. Velázquez, O. E., Weiss, J. and Morency, F. (2017): Preliminary investigation on stall characteristics of a regional BWB for low speed approach. 35th AIAA Applied Aerodynamics Conference, 2017, June, 1–17. https://doi.org/10.2514/6.2017-3738
45. Wisnoe, W., Nasir, R., Kuntjoro, W. and Mamat, A. (2009): Wind Tunnel Experiments and CFD Analysis of Blended Wing Body (BWB) Unmanned Aerial Vehicle (UAV) at Mach 0.1 and Mach 0.3. International Conference on Aerospace Sciences and Aviation Technology, 13(Aerospace Sciences), 1–15. https://doi.org/10.21608/asat.2009.23441